Modeling Glioma Growth and Mass Effect in 3D MR Images of the Brain

Cosmina Hogea[1], Christos Davatzikos[1], and George Biros[2]

[1] Section of Biomedical Image Analysis, Department of Radiology, University of Pennsylvania, Philadelphia PA 19104, USA
[2] Departments of Mechanical Engineering and Applied Mechanics, Bioengineering, and Computer and Information Science, University of Pennsylvania, Philadelphia PA 19104, USA
hogeac@uphs.upenn.edu

Abstract. In this article, we propose a framework for modeling glioma growth and the subsequent mechanical impact on the surrounding brain tissue (mass-effect) in a medical imaging context. Glioma growth is modeled via nonlinear reaction-advection-diffusion, with a two-way coupling with the underlying tissue elastic deformation. Tumor bulk and infiltration and subsequent mass-effects are not regarded separately, but captured by the model itself in the course of its evolution. Our formulation is fully Eulerian and naturally allows for updating the tumor diffusion coefficient following structural displacements caused by tumor growth/infiltration. We show that model parameters can be estimated via optimization based on imaging data, using efficient solution algorithms on regular grids. We test the model and the automatic optimization framework on real brain tumor data sets, achieving significant improvement in landmark prediction compared to a simplified purely mechanical approach.

1 Introduction

Modeling brain tumor growth in conjunction with deformable registration algorithms can be used to construct brain tumor atlases and potentially assist treatment planning [1, 2]. In order to improve registration between a normal brain atlas and a tumor-bearing brain image, it is desirable to first construct a brain atlas exhibiting tumor and mass-effect[1] similar to those of a patient at study, thus reducing the problem to the (simpler) problem of registering two relatively similar images.

Therefore, we need a way to simulate tumor growth and mass-effects for different brain anatomies. In [1,3,4], a purely mechanical 3D tumor growth model targeted on simulations of tumor mass-effect was employed. The brain tissue was modeled as an elastic material (linear or nonlinear) and the mechanical force exerted by the growing tumor was approximated by a constant outward pressure P acting on the tumor boundary and controlling the tumor size and mass-effect. This model was solved to obtain brain tissue displacements. Although this

[1] Deformation (compression) of the neighboring tissue induced by tumor growth is commonly referred to as mass-effect.

N. Ayache, S. Ourselin, A. Maeder (Eds.): MICCAI 2007, Part I, LNCS 4791, pp. 642–650, 2007.

approach was employed successfully for generating tumor-deformed brain atlases, it has two main limitations: (1) more irregularly shaped tumors are difficult to capture (the simulated tumors are generally quasi-spherical); and (2) it provides no information about the actual tumor evolution and infiltration into healthy tissue. In [2], the authors have used a relatively similar mechanical approach to model the mass-effect caused by the tumor bulk (GTV1) and added a separate reaction-diffusion model (similar to [5], [6], [7]) to account for the tumor infiltrative part only (GTV2, assumed to cause little mass-effect). In such an approach, the tumor reaction-diffusion equation is decoupled from the elasticity equations and the diffusion coefficient, which in reality is affected by tumor infiltration, is not updated [2].

Here, we propose a model that strongly couples glioma[2] growth with the subsequent deformation of the brain tissue. Using brain tumor MRI scans, model parameters can be estimated via a biophysically-constrained optimization formulation of a deformable image registration problem. In our approach, glioma growth is modeled via a nonlinear reaction-advection-diffusion equation, with a two-way coupling with the underlying tissue elasticity equations. Our formulation (fully Eulerian) naturally allows for updating the tumor diffusion coefficient following structural displacements caused by tumor growth/infiltration. The overall modeling framework results in a strongly coupled nonlinear system of partial differential equations, for which we use an efficient numerical solution procedure.

The main differences compared to the work in [2] are: (1) there is no sharp-interface separation between a tumor bulk and an infiltrative part; (2) the underlying tissue displacement (deformation) impacts the subsequent motion of the tumor cells in two ways: the diffusion coefficient changes (diffusion term in the tumor equation) and tumor cells are pushed around (advective term in the tumor equation); (3) the diffusion coefficient, affected by structural displacements following tumor growth and infiltration, is updated; (4) the numerical solution algorithm is based on fast hybrid finite element-finite difference solvers on fixed regular grids, coupled with an optimization algorithm for estimation of model parameters from patient imaging data.

2 Methods

The brain is regarded as a deformable solid occupying a bounded region ω in space. Let $U = \omega \times (0, T)$, where $(0, T)$ a specified time interval. Let $c = c(\mathbf{x}, t)$ be the tumor-cell density, normalized such that $0 \leq c \leq 1$. Using an Eulerian frame of reference, the tumor growth and the subsequent brain motion can be described by the following general set of equations:

$$\frac{\partial c}{\partial t} - \nabla \cdot (D \nabla c) + \nabla \cdot (c\mathbf{v}) - \rho c(1 - c) = 0 \tag{1}$$

$$\nabla \cdot ((\lambda \nabla \cdot \mathbf{u})\mathbf{I} + \mu(\nabla \mathbf{u} + \nabla \mathbf{u}^T)) - p_1 e^{-\frac{p_2}{c^s}} e^{-\frac{p_2}{(2-c)^s}} \nabla c = 0 \tag{2}$$

$$\mathbf{v} = \frac{\partial \mathbf{u}}{\partial t}, \qquad \frac{\partial \mathbf{m}}{\partial t} + (\nabla \mathbf{m})\mathbf{v} = 0, \tag{3}$$

[2] Malignant gliomas are the most common primary brain tumors, originating in the glial cells; they are often resistant to treatment and carry a poor prognosis.

where $\mathbf{m} = (\lambda, \mu, D)$. In regions where $c \ll 1$ (infiltration), the customary proliferation term ρc corresponding to exponential growth at rate ρ is retrieved [5]. Proliferation is assumed to slow down in regions with c getting closer to 1 (tumor bulk), and it eventually becomes a death term if c becomes larger than 1[3]; D is the diffusion coefficient of tumor cells in brain tissue[4]. Here we consider the case of isotropic diffusion in both white and gray matter, with diffusion coefficients D_w and D_g, respectively [5]. $\mathbf{v}$ is the (Eulerian) velocity field[5], $\mathbf{u}$ is the displacement field.

We employ the linear elasticity theory and approximate the brain tissue as a linear elastic material, characterized by Lame's parameters λ and μ (related to Young's modulus E and Poisson's ratio ν). The elastic forces are pressure-like, directly proportional to the local gradient of the tumor cell density [9], [2]; the expression we use here, with p_1, p_2 and s positive constants, allows for flexibility in capturing both strong tumor mass-effect (generally caused by the tumor bulk) and milder mass-effects (generally caused by tumor infiltration), as illustrated in figure 1. The elastic material properties λ and μ and the tumor cell diffusivity D are assumed spatially varying (different in white matter, gray matter, ventricles, CSF). Boundary and initial conditions are specified to close the system of equations (1)-(3). We impose zero tumor cell flux and zero tissue displacement at the skull. The advection equations (3) are initial value problems, with the initial values assigned from the corresponding segmented MR image [3,4]. Equations (1)-(3) with prescribed boundary and initial conditions represent a mixed parabolic-elliptic-hyperbolic nonlinear system of PDEs. Next, we outline an efficient numerical algorithm for solving this system.

2.1 Numerical Methods

A significant challenge is posed by the fact that the underlying spatial domain ω occupied by the brain is a highly irregular one. Various techniques exist for solving PDEs on an irregular domain, from unstructured meshes that conform to the irregular domain boundary to immersed interface/ghost-fluid methods. Here, we employ a fictitious domain-like regular grid method. The target domain ω is embedded on a larger computational rectangular domain (box) Ω. The PDEs originally defined on ω, are appropriately extended to Ω, such that the true boundary conditions prescribed on $\partial\omega$ are approximated.

For simplicity, it is advantageous to split the problem into independent steps corresponding to the advection, diffusion, and reaction [10], [11]. Let $\mathbf{w} = (c, \mathbf{u}, \mathbf{v}, D, \lambda, \mu)$ denote the vector of unknowns. Let Δ, A_1, and R denote the diffusion, advection and reaction operators in the diffusion equation (1), and A_2 denote the advection operator in equations (3). Let $\mathbf{w}^n = (c^n, \mathbf{u}^n, \mathbf{v}^n, D^n, \lambda^n, \mu^n)$ is the solution at time $t = t_n$; to update the solution $\mathbf{w}^{n+1}$ at the next time step $t_{n+1} = t_n + \Delta t$ we use three steps.

[3] We do model tumor as a single species and we ignore heterogeneity.

[4] If tumor diffusion is assumed anisotropic, then D is a tensor.

[5] The velocity $\mathbf{v}$ in the tumor equation may well depend on tumor specific mechanisms (e.g., chemotaxis [8]). In our model the velocity accounts only for the tumor cells being displaced as a consequence of the underlying tissue mechanical deformation.

(I) We solve the advection equations (3) over time Δt to obtain $(D^{n+1}, \lambda^{n+1}, \mu^{n+1})$;
(II) We solve the diffusion equation (1) using a simple fractional step method [10]: a) Solve $\frac{\partial c}{\partial t} = A_1(c, \mathbf{v})$ over time Δt with data $(c^n, \mathbf{v}^n)$ to obtain c^*;
b) Solve $\frac{\partial c}{\partial t} = \Delta(c, D)$ over time Δt with data (c^*, D^{n+1}) to obtain c^{**};
and c) Solve $\frac{\partial c}{\partial t} = R(c)$ over time Δt with data c^{**} to obtain c^{n+1}.
(III) Finally, we solve the elasticity equation (2) with data $(c^{n+1}, \lambda^{n+1}, \mu^{n+1})$ to obtain $\mathbf{u}^{n+1}$ and update the velocity $\mathbf{v}^{n+1}$.

Parameter estimation (optimization)
Consider the case of longitudinal data for a brain-tumor subject. We seek to compute the model parameters that generate images that 'best match' the patient data. This translates into a parameter-estimation problem for the model governing equations (1)-(3). Here we use an objective functional that defines a 'best match' by the Euclidean distance between model-generated landmarks and manually-placed landmarks in the target image(s). The results presented in the next section are obtained using the APPSPACK package [12], a derivative-free optimization library from Sandia National Laboratory. More efficient optimization algorithms, based on gradient estimation via the adjoints [13], are work in progress.

3 Results

Given the segmented image labels (generated from 3D MRI data), we assign piecewise constant material properties (white matter, gray matter, ventricles, and CSF). These values are used as initial condition in the transport equations (3). The 3D computational domain is the underlying domain of the image. It consists of the actual brain plus the surrounding fictitious material.

Synthetic brain tumor images
We first illustrate the capabilities of our proposed framework to simulate brain tumors with more complex patterns and mass-effect. For the simulations in Figure 1 we have used similar values for the elastic material properties as in [3, 4]. The tumor diffusivity in the white matter was set five times higher than in the gray matter [5], while the diffusivity in the ventricles (and eventually CSF) was set to zero. These simulations correspond to an aggressive physical tumor growth over T=365 days (one year), starting from the same small Gaussian seed located in the right frontal lobe. The numerical solution of our coupled system of PDEs (1)-(3) is obtained via the procedure described in section 2.1 using a hybrid finite element-finite difference method, with ten equal time steps and a spatial discretization of $65 \times 65 \times 65$ nodes[6]. The tumor growth illustrated in the second column (left to right) of figure 1 is less diffusive ($D_w = 7.5 \times 10^{-8} m^2/day; D_g = 1.5 \times 10^{-8} m^2/day$) and more regularly shaped, while in the other two case scenarios depicted in the third and fourth

[6] By extensive numerical testing, we have found that such a discretization provides a reasonable trade-off between speed and accuracy.

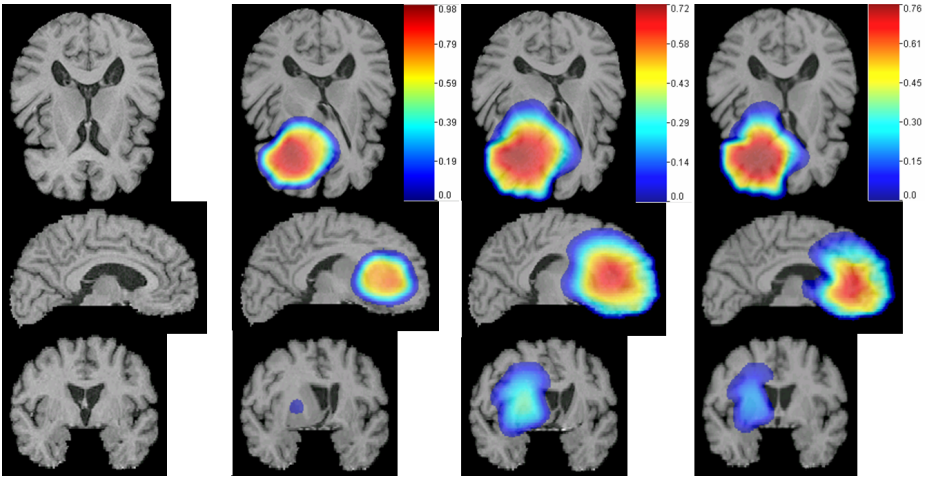

Fig. 1. Synthetic glioma growth, right frontal lobe: three different case scenarios starting from the same initial tumor seed. Left to right. The 1st column illustrates the 3D MRI of a normal brain image—axial, sagittal and coronal section respectively. The 2nd column shows the deformed image, with simulated tumor corresponding to low tumor diffusivity and long-range mass-effect ($p_2 = 0$). The 3rd column shows the deformed image, with simulated tumor corresponding to high tumor diffusivity (ten times higher) and long-range mass-effect ($p_2 = 0$). Finally, the 4th column shows the deformed image, with simulated tumor corresponding to high tumor diffusivity and short-range mass-effect ($p_2 = 0.1$). The tumor maps (here shown in RGB) are overlaid on the deformed template. The run time is about 500 seconds on an 2.2GHz AMD Opteron.

column (left to right) respectively, we increased the diffusivity by a factor of ten ($D_w = 7.5 \times 10^{-7} m^2/day; D_g = 1.5 \times 10^{-7} m^2/day$). For both simulations illustrated on the second and third columns (left to right) of figure 1, the parameter p_2 regulating the range of the mass-effect was set equal to zero, which is the minimum, corresponding to an extreme case scenario, with strong mass-effects propagating far away from the tumor core, which we refer to as 'long-range' mass-effects. This can be well observed by examining the ventricle deformation in the corresponding axial slices. If p_2 is increased, the mass-effects are more localized to areas close to the tumor core, which can be well observed on the fourth column of figure 1 and which we refer to as 'short-range' mass-effects. The rest of the model parameters are kept fixed to $\rho = 0.036/day, p_1 = 15kPa, s = 2$. More complex tumor patterns could be obtained by using more complicated initial tumor profiles and/or anisotropic diffusion (DTI-driven).

Optimization on real brain tumor data and comparison with simpler pressure-based mechanical model

In [3,4], the authors have investigated the ability of their proposed framework to realistically capture mass-effects caused by actual brain tumors in two dog cases with surgically transplanted glioma cells and a human case with progressive low-grade glioma. We use their data sets here for comparison purposes. For the two

Table 1. Landmark errors for the two dog cases (DC1, DC2) and for the human case (HC) with the new model (optimized). The errors shown are with respect to landmarks manually placed by an experienced human rater. Both the incremental pressure model and the new model were numerically solved using a spatial discretization with 65^3 nodes; five equal pressure increments applied in the simple pressure model; four equal time steps used in the new model for the two dog cases and five equal time steps for the human case.

Landmark Error (mm)	Median	Min	Max	Run time (sec)
New model DC1	**0.89564**	**0.0511**	**1.9377**	**200**
Incremental pressure model	**1.6536**	**0.3176**	**2.6491**	**300**
Inter-rater variability DC1	**0.8484**	**0.1304**	**2.8568**	
New model DC2	**1.2980**	**0.3803**	**2.6577**	**200**
Incremental pressure model	**1.8912**	**0.4795**	**3.7458**	**300**
Inter-rater variability DC2	**1.3767**	**0.1226**	**2.7555**	
New model HC	**1.8457**	**0.5415**	**4.1451**	**250**
Incremental pressure model	**5.23**	**1.15**	**8.9**	**300**

dogs (DC1, DC2), a baseline scan was acquired before tumor growth, followed by scans on the 6th and 10th day post-implantation. Gadolinium-enhanced T1 MR images were acquired. By the 10th day, tumors grew rapidly to a diameter of 1-2 cm, and then the animals were sacrificed (prior to any neurological complications). For the human case (HC), two T1 MRI scans with approximately 2.5 years in-between were available. In all three cases, pairs of corresponding landmark points were manually identified by human raters in the starting and target images. For the dog cases, two human raters placed independent sets of landmarks. All the results reported here are with respect to the most experienced rater of the two; the inter-rater variability is included in table 1.

For the human case, only one human rater was available. We have fixed the elastic material properties (stiffness and compressibility, respectively) to the values reported in [3, 4][7]. We consider a case-scenario with four optimization parameters: c_0, D_w, ρ, p_1 (p_2 fixed to zero). Here c_0 represents a scaling factor (magnitude) of the initial tumor density, assumed again to be a Gaussian with known center (here estimated from the serial scans). The landmark errors upon optimization convergence are summarized in table 1; corresponding landmark errors for the simplified purely mechanical approach in [3, 4] are included for comparison. Relative landmark errors with respect to the maximum landmark displacement for both the simplified incremental pressure approach [3, 4] and the new model are shown for comparison in figure 2; the corresponding average relative improvement achieved by the new (optimized) model are 17%, 20% and 51% for DC1,DC2 and HC, respectively. A visual illustration of simulations via the two different approaches (new model vs. incremental pressure) is shown in figure 3 (top row), highlighting the potential of the new model to capture more information about the tumor compared to the pressure approach.

[7] In these three cases, the segmentation included only white matter and ventricles: $E_{white} = 2100Pa, E_{ventricles} = 500Pa, \nu_{white} = 0.45, \nu_{ventricles} = 0.1$

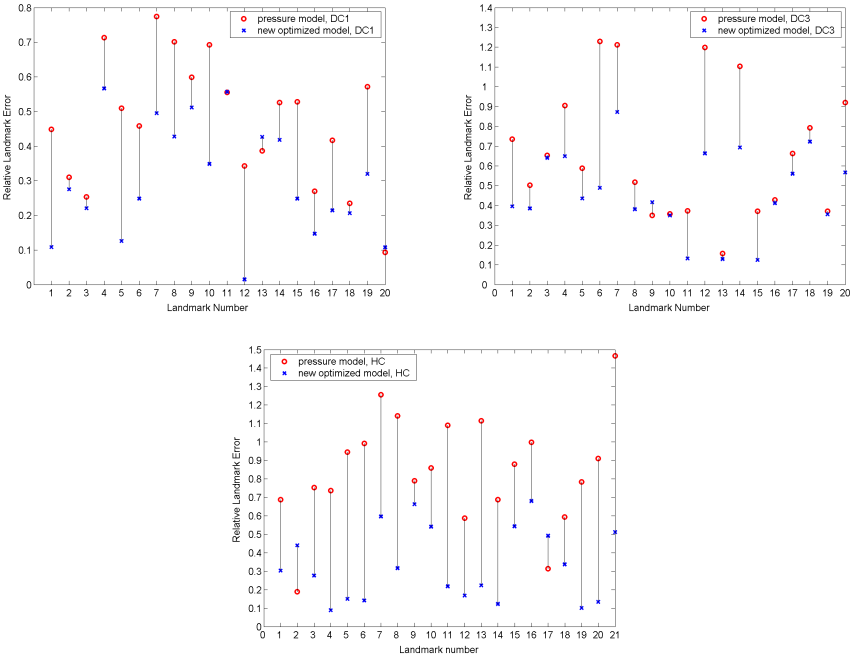

Fig. 2. Comparison of relative landmark errors (here with respect to the maximum landmark displacement) for the three cases DC1, DC2 and HC, via the the incremental pressure approach and the new model. The corresponding average relative improvements achieved by the new optimized model are 17%, 20% and 51% for DC1,DC2 and HC, respectively.

4 Conclusions and Further Research

In the present paper, we proposed a framework for modeling gliomas growth and the subsequent mass-effect on the surrounding brain tissue. Estimation of unknown model parameters is regarded as a constrained optimization problem. Although beyond the scope of the current paper, the long-term aims of this work are the following goals: to improve the deformable registration from a brain tumor patient image to a common stereotactic space (atlas) with the ultimate purpose of building statistical atlases of tumor-bearing brains; to investigate predictive features for glioma growth, after the model parameters are estimated from given patient scans. We illustrated the capabilities and flexibility of our new framework in capturing more complex/realistic tumor shapes and subsequent mass-effect, at reduced computational cost. We tested both the model and the optimization framework on real brain tumor data sets and showed significant improvement compared to a simplified purely mechanical approach [3, 4]. We are currently working on developing faster PDE-constrained optimization methods, with estimation of gradients via an adjoint-based formulation coupled to fast gradient-descent algorithms and general image similarity functionals.

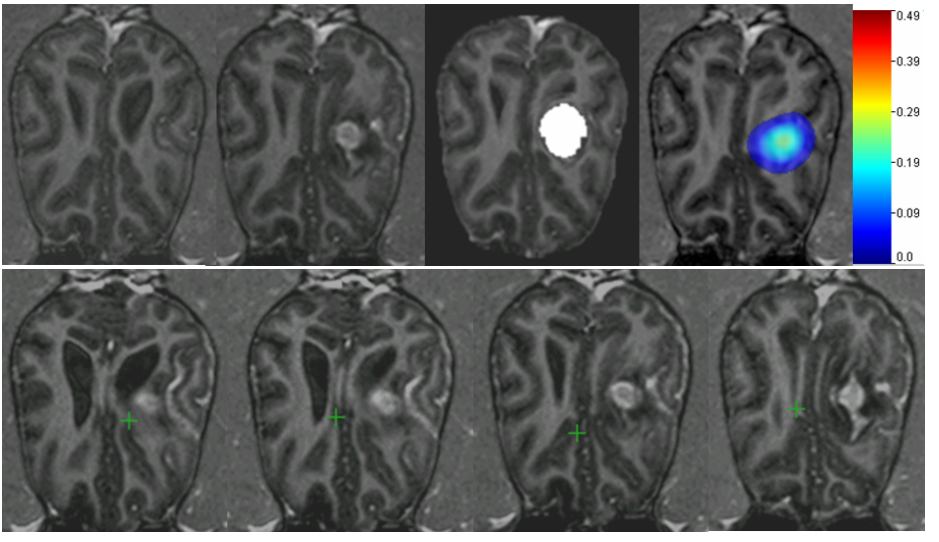

Fig. 3. Real brain tumor images, dog case DC1. ***Top row***, from left to right: starting scan, T1 MR gadolinium-enhanced; target scan, T1 MR gadolinium-enhanced; our simulated tumor growth and mass-effect via the new optimized framework: tumor color maps overlaid on the model-deformed image, with corresponding color bar attached; simulated mass-effect via the simplified incremental pressure approach in [3], with tumor mask highlighted in white. The new tumor growth model shows potential to capture more information about the tumor compared to the pressure approach. ***Bottom row***: illustration of a few of the target landmarks (marked with crosses) used for the model-constrained optimization in this case.

Finally, we are building non-uniform structured discretizations based on octree data structures to further reduce computational cost and allow more accurate approximations in regions of interest.

References

1. Mohamed, A., Davatzikos, C.: Finite element modeling of brain tumor mass-effect from 3d medical images. In: Proceedings of Medical Image Computing and Computer-Assisted Intervention, Palm Springs (2005)
2. Clatz, O., Sermesant, M., Bondiau, P.-Y., Delingette, H., Warfield, S.K., Malandain, G., Ayache, N.: Realistic simulation of the 3d growth of brain tumors in mr images coupling diffusion with mass effect. IEEE Trans on Med. Imaging 24, 1334–1346 (2005)
3. Hogea, C., Abraham, F., Biros, G., Davatzikos, C.: A framework for soft tissue simulations with applications to modeling brain tumor mass-effect in 3d images. In: Medical Image Computing and Computer-Assisted Intervention Workshop on Biomechanics, Copenhagen (2006)
4. Hogea, C., Abraham, F., Biros, G., Davatzikos, C.: Fast solvers for soft tissue simulation with application to construction of brain tumor atlases (Technical report) ms-cis-07-04, `http://www.seas.upenn.edu/~biros/papers/brain06.pdf`

5. Swanson, K.R., Alvord, E.C., Murray, J.D.: A quantitative model for differential motility of gliomas in grey and white matter. Cell Proliferation 33, 317–329 (2000)
6. Tracqui, P., Mendjeli, M.: Modelling three-dimensional growth of brain tumors from time series of scans. Mathematical Models and Methods in Applied Sciences 9, 581–598 (1999)
7. Habib, S., Molina-Paris, C., Deisboeck, T.: Complex dynamics of tumors: modling an emerging brain tumor system with coupled reaction-diffusion equations. Physica A: Statistical Mechanics and its Applications 327, 501–524 (2003)
8. Hogea, C.: Modeling Tumor Growth: a Computational Approach in a Continuum Framework. PhD thesis, Binghamton University (2005)
9. Wasserman, R.M., Acharya, R.S., Sibata, C., Shin, K.H.: Patient-specific tumor prognosis prediction via multimodality imaging. Proc. SPIE Int. Soc. Opt. Eng. 2709 (1996)
10. Tyson, R., Stern, L.G., LeVeque, R.J.: Fractional step methods applied to a chemotaxis model. J. Math. Biol. 41, 455–475 (2000)
11. Verwer, J., Hundsdorfer, W., Blom, J.: Numerical time integration for air pollution models. In: Report MAS-R9825, CWI Amsterdam (1991)
12. Kolda, T., et. al.: APPSPACK (2005), home page. `http://software.sandia.gov/appspack/version5.0`
13. Gunzburger, M.: Perspectives in Flow Control and Optimization. SIAM (2002)